

ALIGNMENT OF THE SCALAR GRADIENT IN EVOLVING MAGNETIC FIELDS

SHARANYA SUR¹, LIUBIN PAN², & EVAN SCANNAPIECO¹

Draft version March 11, 2022

ABSTRACT

We conduct simulations of turbulent mixing in the presence of a magnetic field, grown by the small-scale dynamo. We show that the scalar gradient field, ∇C , which must be large for diffusion to operate, is strongly biased perpendicular to the magnetic field, \mathbf{B} . This is true both early-on, when the magnetic field is negligible, and at late times, when the field is strong enough to back react on the flow. This occurs because ∇C increases within the plane of a compressive motion, but \mathbf{B} increases perpendicular to it. At late times the magnetic field resists compression, making it harder for scalar gradients to grow and likely slowing mixing.

Subject headings: ISM:abundances - magnetic fields - magnetohydrodynamics (MHD) - turbulence

1. INTRODUCTION

When pollutants are added to a magnetized, turbulent medium, the motions will stretch the concentration field and the magnetic field lines simultaneously. The random stretching of the concentration field causes a cascade to smaller scales, which amplifies scalar gradients and leads to homogenization by molecular diffusivity (Shraiman & Siggia 2000; Pan & Scannapieco 2010; Pan et al. 2013). Random stretching also rapidly grows a weak magnetic field to dynamically important strengths by the action of the small-scale dynamo. In this mechanism, the magnetic field growth is initially exponential, until magnetic back reactions resist stretching and folding of the field lines, resulting in saturation (Schekochihin et al. 2004; Haugen et al. 2004; Brandenburg & Subramanian 2005; Cho et al. 2009; Cho & Ryu 2009; Federrath et al. 2011; Brandenburg et al. 2012; Bhat & Subramanian 2013). Understanding mixing in the presence of such evolving magnetic fields is crucial for astrophysical flows in diverse environments, as mixing plays a vital role in intergalactic enrichment (Schaye et al. 2003; Pichon et al. 2003; Pieri et al. 2006; Scannapieco et al. 2006; Becker et al. 2009), thermal conduction in the magnetized intracluster gas (Komarov et al. 2014), the dispersion of heavy elements in the interstellar medium (Pan & Scalo 2007), and pollution of the pristine gas in the early Universe (Pan et al. 2013).

In an earlier work (Sur et al. 2014), we reported on direct numerical simulations of scalar mixing in the presence of an evolving magnetic field, generated by the small-scale turbulent dynamo. One of the important results obtained in that study was the fact that scalar

mixing is hindered by dynamically important magnetic fields, leading to longer mixing time scales. However, some key questions concerning the mechanism by which mixing is slowed remained unanswered. Mixing occurs by molecular diffusion in directions of strong concentration gradients, gradients that are built up by the same turbulent motions that cause magnetic field amplification. Thus an important, open question is the degree to which the directions of magnetic fields and concentration gradients are aligned. In the context of galaxy clusters, Komarov et al. (2014) found that random motions suppress local thermal conduction by aligning the magnetic fields transverse to the local temperature gradient. Similarly, how such alignments evolve over the kinematic and saturated phases of magnetic field evolution is likely to have strong consequences for the efficiency of fluid mixing as occurs in a wide variety of astrophysical environments.

The purpose of this *Letter* is to dwell upon these concerns and develop a coherent physical picture of passive scalar mixing in a turbulent, magnetized medium. To this end, we analyze the data of a subset of simulations reported in (Sur et al. 2014), where we performed a suite of numerical simulations of this process using the publicly available MHD code FLASH (Fryxell et al. 2000). For the aims and scope of this contribution, we will focus on the alignments of the magnetic field, the vorticity, and the scalar gradient, encompassing both the kinematic and nonlinear phases of magnetic field evolution, which as we will show, provides a unique perspective on the underlying physics of both turbulent mixing and dynamo action. This Letter is organized as follows. In Section 2, we briefly describe our numerical methods and initial conditions. The results obtained from our study and an overview of the overall physical picture they suggest are presented in Section 3.

2. NUMERICAL MODELING

The details of the numerical setup are described in Sur et al. (2014). In the following, we only highlight the

sharanya.sur@asu.edu, lpan@cfa.harvard.edu,
evan.scannapieco@asu.edu

¹School of Earth and Space Exploration, Arizona State University, PO Box 876004, Tempe - 85287, USA

²Harvard-Smithsonian Center for Astrophysics, 60 Garden St., Cambridge MA 02138, USA

essential features of our simulations. We adopted an isothermal equation of state, a uniform 512^3 grid with periodic boundary conditions, and velocities driven by solenoidal modes at about half the scale of the box. Mixing was studied by tracking the evolution of a scalar concentration field, $C(\mathbf{x}, t)$, i.e., the local mass fraction of pollutants, driven on the same scale as the velocities (Pan & Scannapieco 2010; Sur et al. 2014), with homogenization most efficient in regions in which the scalar gradient, ∇C , is large. In all simulations, the initial magnetic field was uniform, pointed in the z -direction, with plasma beta $\beta \equiv 2p/B^2 = 10^7$, where p is the thermal pressure and B is the magnetic field strength.

We primarily examine a non-ideal run with a Mach number $\mathcal{M} = 0.3$, Prandtl and Schmidt numbers $\text{Pm} = \text{Sc} = 1$, and a fluid Reynolds number $\text{Re} = 1250$, defined as the ratio of the product of the forcing scale of the turbulence and the three-dimensional velocity dispersion to the viscosity. In addition, we also consider two ideal runs at $\mathcal{M} = 0.3$ and $\mathcal{M} = 2.4$. In these runs, the dissipation of kinetic and magnetic energies as well as the scalar variance is through numerical diffusion, and thus the effective magnetic Prandtl and Schmidt numbers are both of $\approx O(1)$. We use the unsplit staggered mesh algorithm in FLASHv4 with a constrained transport scheme to maintain $\nabla \cdot \mathbf{B}$ to machine precision (Lee & Deane 2009; Lee 2013) and the HLLD Riemann solver (Miyoshi & Kusano 2005), instead of artificial viscosity to capture shocks. In the context of studying the nature of the alignments, the motivation for including these ideal runs is twofold - to explore if the qualitative nature of the alignments is sensitive to the presence or absence of explicit physical dissipation and secondly, to study the effect of compressibility.

3. RESULTS

3.1. Scalar Gradients, Magnetic Fields, and Vorticity

In Figure 1, we show three-dimensional volume renderings of the projections of the directional unit vectors of the magnetic field ($\mathbf{n}_B \equiv \mathbf{B}/|\mathbf{B}|$), the vorticity ($\mathbf{n}_\omega \equiv \boldsymbol{\omega}/|\boldsymbol{\omega}|$), and the scalar gradient ($\mathbf{n}_{\text{gc}} \equiv \nabla C/|\nabla C|$) for the non-ideal $\mathcal{M} = 0.3$ and ideal $\mathcal{M} = 2.4$ runs. For the subsonic run, we show both the kinematic and saturated phases of magnetic field evolution at times $t = 2.5 t_{\text{ed}}$ and $8.8 t_{\text{ed}}$ respectively, while for the supersonic run we show only the saturated phase at $t = 22 t_{\text{ed}}$. Here t_{ed} is the eddy-turnover time. The saturated values of the magnetic to kinetic energies are ≈ 0.36 for the subsonic run and ≈ 0.16 for the supersonic run. As evident from the figure, in both kinematic and the saturated phases and for both $\mathcal{M} = 0.3$ and 2.4 , a positive correlation between \mathbf{n}_B and \mathbf{n}_ω is evident, whereas, \mathbf{n}_{gc} appears to align transversely to both \mathbf{n}_ω and \mathbf{n}_B .

To quantify these visual impressions, we show in Figure 2 the probability distribution functions (PDFs) of the cosines of the angles between the three vectors in all three simulations considered here. For the two subsonic runs, the PDFs are averaged over $t = (1.5 - 4) t_{\text{ed}}$

in the kinematic phase and over $t = (6 - 9) t_{\text{ed}}$ in the saturated phase. For $\mathcal{M} = 2.4$, they are averaged over $t = (3 - 9) t_{\text{ed}}$ and $t = (21 - 25) t_{\text{ed}}$ respectively. In all runs, and in both the kinematic and saturated phases, the direction of the scalar gradient tends to be orthogonal to the magnetic field, implying that scalar dissipation occurs primarily perpendicular to \mathbf{n}_B . The figure also confirms that magnetic field and vorticity are aligned in the two phases. Such a correlation was also observed in Brandenburg et al. (1995); Miller et al. (1996), although the degree of alignment decreases once the magnetic field attains saturation. In the kinematic phase, we find that there is a strong tendency of the scalar gradient to be perpendicular to the vorticity Ashurst et al. (1987); Kerr (1987), which also becomes weaker in the saturated phase. Apart from minor differences, it is evident that the alignment of the three unit vectors is qualitatively independent of the flow compressibility and the presence or absence of explicit dissipative terms.

Insight into these alignments can be gained from the evolution equations of \mathbf{B} , ∇C , and $\boldsymbol{\omega}$. The magnetic and scalar fields are deformed by the velocity gradient $\partial u_i/\partial x_j$, which can be decomposed into a rate of strain tensor $\mathcal{S}_{ij} \equiv (\partial u_i/\partial x_j + \partial u_j/\partial x_i)/2 - (\partial_k u_k)\delta_{ij}/3$, a rate of expansion tensor, $(\partial_k u_k)\delta_{ij}/3$, and an antisymmetric tensor $\Omega_{ij} \equiv \epsilon_{ijk}\omega_k/2$, corresponding to the vorticity. From the magnetic induction and the scalar equations, we have,

$$\frac{D\mathbf{B}}{Dt} = \mathbf{B} \cdot \boldsymbol{\mathcal{S}} - \frac{2}{3}(\nabla \cdot \mathbf{u})\mathbf{B} - \frac{1}{2}(\mathbf{B} \times \boldsymbol{\omega}) + \eta \nabla^2 \mathbf{B}, \quad (1)$$

and

$$\frac{D\nabla C}{Dt} = -\nabla C \cdot \boldsymbol{\mathcal{S}} - \frac{1}{3}(\nabla \cdot \mathbf{u})\nabla C - \frac{1}{2}(\nabla C \times \boldsymbol{\omega}) + \kappa \nabla^2(\nabla C), \quad (2)$$

where D/Dt is the Lagrangian derivative, and η and κ are the resistivity and diffusivity, respectively.³ In the above equations, the terms proportional to $\boldsymbol{\omega}$ correspond to the simultaneous rotation of \mathbf{B} and ∇C by the vorticity, which leave their magnitudes unchanged. However, the divergence terms may change the amplitudes of \mathbf{B} and ∇C , but not their directions. Instead, it is the strain that continuously amplifies both \mathbf{B} and ∇C and determines their relative orientation. Flux-freezing suggests that \mathbf{B} increases normal to compressive directions of the strain, but ∇C is amplified along the compressive directions. Therefore, the directions of \mathbf{B} and ∇C always tend to be perpendicular, as seen in Figure 2. Such an orthogonal orientation in the kinematic phase was also reported by Komarov et al. (2014), in the context of thermal conduction in galaxy clusters, where it leads to a suppression of the thermal flux.

Ignoring the large-scale driving force, the vorticity

³ For simplicity, we ignored the spatial fluctuations of η , κ , and the density, which would cause extra terms like $(\nabla^2 C)\nabla \kappa$. A similar situation occurs for eq. 3 below.

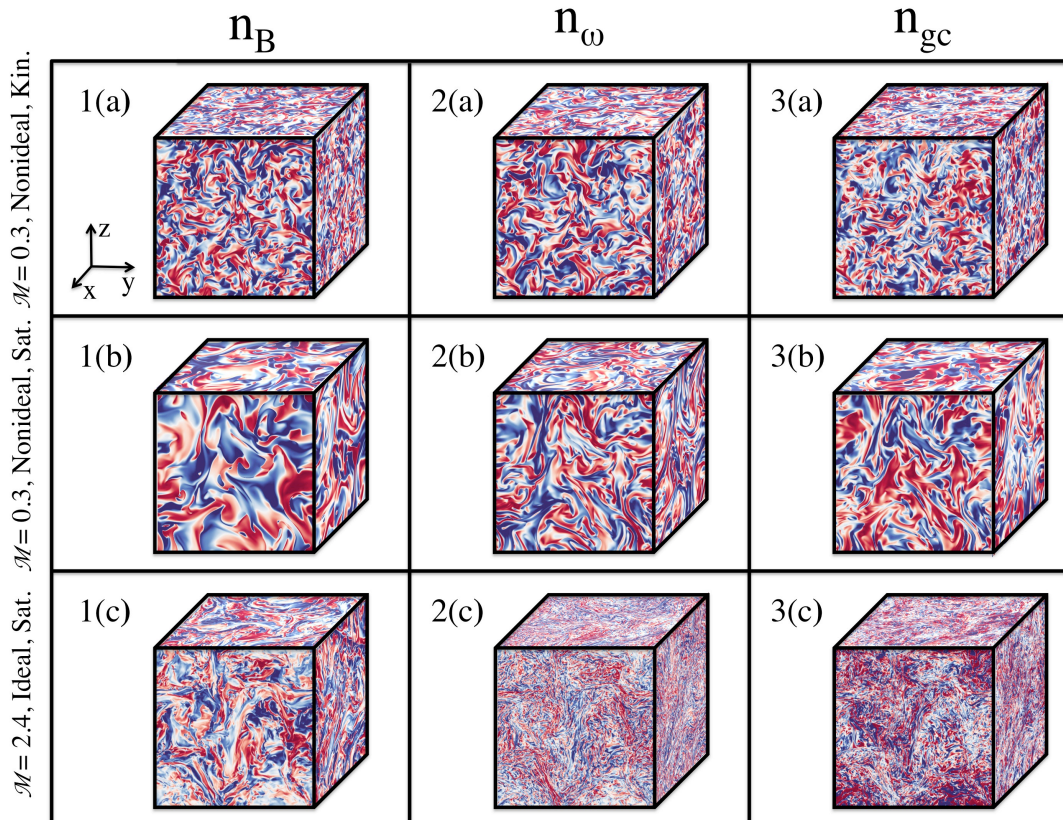


Figure 1. Three-dimensional rendering of the projection of unit vectors of the magnetic field (\mathbf{n}_B), the vorticity (\mathbf{n}_ω), and the scalar gradient (\mathbf{n}_{gc}). The first and second rows correspond to the kinematic and saturated phases of the magnetic evolution for the non-ideal $\mathcal{M} = 0.3$ runs at $t/t_{ed} = 2.5$ and 8.8 respectively. The last row shows the saturated phase of the ideal $\mathcal{M} = 2.4$ run at $t/t_{ed} = 22$. Blue denotes vectors pointing outwards, red denotes vectors pointing inwards, and white denotes vectors along the faces.

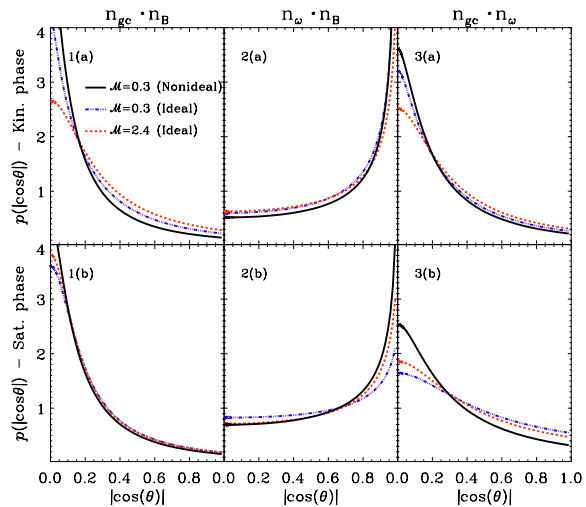


Figure 2. PDFs of the alignments of \mathbf{n}_B , \mathbf{n}_{gc} and \mathbf{n}_ω in the kinematic (upper row) and saturated phase (lower row) of magnetic field amplification. The data correspond to the $\mathcal{M} = 0.3$ (black solid) and 2.4 (red dashed) ideal runs, and a non-ideal $\mathcal{M} = 0.3$ (blue dash-dotted) run.

equation reads,

$$\frac{D\boldsymbol{\omega}}{Dt} = \boldsymbol{\omega} \cdot \boldsymbol{\mathcal{S}} - \frac{2}{3} (\nabla \cdot \mathbf{u}) \boldsymbol{\omega} + \frac{\nabla \rho \times \nabla p}{\rho^2} + \nabla \times \mathbf{L} + \nu \nabla^2 \boldsymbol{\omega}, \quad (3)$$

where p is the thermal pressure, and $\mathbf{L} = \mathbf{J} \times \mathbf{B}/\rho$ is the acceleration by the Lorentz force with $\mathbf{J} = \nabla \times \mathbf{B}/4\pi$ the current density. In our isothermal simulations, the baroclinic term vanishes, and \mathbf{L} is negligible in the kinematic phase. Similar to the evolution of \mathbf{B} , the divergence term in equation 3 does not influence the direction of $\boldsymbol{\omega}$, but the strain amplifies $\boldsymbol{\omega}$ in the extensive or stretching direction(s). Due to angular momentum conservation, a compression by the strain leads to an increase in the vorticity in the normal direction (Ashurst et al. 1987). In the saturated phase, the Lorentz effect becomes important, causing a weaker alignment of $\boldsymbol{\omega}$ with \mathbf{B} and weaker orthogonal orientation with ∇C , as seen in Figure 2. Interestingly, we also find the direction of \mathbf{L} is strongly aligned with \mathbf{n}_{gc} in both the kinematic and saturated phases, indicating that one effect of the Lorentz force is to oppose compression. This is related to the buildup of the magnetic pressure gradient along the compressive direction(s) of the strain.

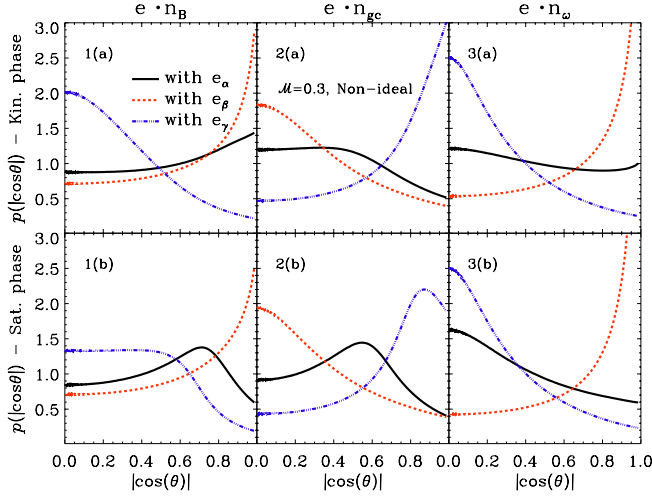


Figure 3. PDFs of the alignments of \mathbf{n}_B , \mathbf{n}_{gc} and \mathbf{n}_w with eigenvectors of \mathbf{S} for the non-ideal $\mathcal{M} = 0.3$ run in the kinematic (upper row) and saturated phase (lower row), respectively. Black solid, red dashed, and blue dash-dotted lines denote alignments w.r.t to \mathbf{e}_α , \mathbf{e}_β and \mathbf{e}_γ , respectively.

3.2. Strain Tensor

As the amplifications of \mathbf{B} , $\boldsymbol{\omega}$, and ∇C all depend on the strain tensor, \mathbf{S} , an analysis of their orientations with respect to the eigenvectors of \mathbf{S} sheds further physical insight into the problem. We denote the eigenvectors of \mathbf{S} by \mathbf{e}_α , \mathbf{e}_β , and \mathbf{e}_γ , corresponding to the eigenvalues $\alpha > \beta > \gamma$, respectively, with $\alpha + \beta + \gamma = 0$. Thus, \mathbf{e}_α and \mathbf{e}_γ correspond to the directions of stretching and compression respectively, and the intermediate eigenvector \mathbf{e}_β has been found to be generally extensive (Ashurst et al. 1987).

The evolution of the eigenvalues and eigendirections can be derived from the equation for the strain tensor,

$$\begin{aligned} \frac{D\mathbf{S}}{Dt} = & -\mathbf{S} \cdot \mathbf{S} + \frac{\mathbf{S} : \mathbf{S}}{3} \mathbf{I} - \frac{1}{4}(\boldsymbol{\omega}\boldsymbol{\omega} - \frac{\boldsymbol{\omega}^2}{3} \mathbf{I}) \\ & - \frac{2}{3}(\nabla \cdot \mathbf{u})\mathbf{S} - \mathcal{P} + \frac{\text{tr}(\mathcal{P})}{3} \mathbf{I} + \mathcal{L}, \end{aligned} \quad (4)$$

where \mathbf{I} is the unit tensor, $\mathcal{P} = \nabla(\nabla p/\rho)$ is the thermal pressure hessian, $\mathcal{L}_{ij} = (\partial L_i/\partial x_j + \partial L_j/\partial x_i)/2 - \partial_k L_k \delta_{ij}/3$, and the viscous term is omitted for simplicity. The terms proportional to \mathbf{I} ensure that \mathbf{S} is traceless while the vorticity term is related to a centrifugal effect that tends to produce an expansion perpendicular to $\boldsymbol{\omega}$. The $-2(\nabla \cdot \mathbf{u})\mathbf{S}/3$ term suggests that local compressions (expansions) by compressible modes in a supersonic flow may amplify (reduce) the amplitude of \mathbf{S} . In the coordinate system of local eigenvectors, equation 4 suggests that the eigenvalues of \mathbf{S} are affected by the diagonal components of the tensors on the right hand side, while the off-diagonal components cause the rotation of the eigenvectors. For example, a calculation of

$\mathbf{e}_\alpha \cdot D\mathbf{S}/Dt \cdot \mathbf{e}_\beta$ using equation 4 yields,

$$\frac{D\mathbf{e}_\alpha}{Dt} \cdot \mathbf{e}_\beta = -\frac{1}{\alpha - \beta} \left(\frac{\boldsymbol{\omega}_\alpha \boldsymbol{\omega}_\beta}{4} + \mathcal{P}_{\alpha\beta} - \mathcal{L}_{\alpha\beta} \right), \quad (5)$$

where $D\mathbf{e}_\alpha/Dt \cdot \mathbf{e}_\beta$ corresponds to the projection of the directional change of \mathbf{e}_α onto the \mathbf{e}_β direction, $\mathcal{P}_{\alpha\beta} = \mathbf{e}_\alpha \cdot \mathcal{P} \cdot \mathbf{e}_\beta$ and $\mathcal{L}_{\alpha\beta} = \mathbf{e}_\alpha \cdot \mathcal{L} \cdot \mathbf{e}_\beta$ (Nomura & Post 1998). Similar equations can be derived for $D\mathbf{e}_\beta/Dt \cdot \mathbf{e}_\gamma$ and $D\mathbf{e}_\gamma/Dt \cdot \mathbf{e}_\alpha$.

In Figure 3, we plot the PDFs of the cosines of the angles between \mathbf{n}_B , \mathbf{n}_{gc} , \mathbf{n}_w , and the three eigenvectors of \mathbf{S} for the non-ideal $\mathcal{M} = 0.3$ flow. Similar results were obtained for the ideal runs with $\mathcal{M} = 0.3$ and 2.4. This similarity suggests that the compressible modes do not significantly affect the relative directions of the vectors considered here. While it is clear that the divergence term leaves the directions of \mathbf{n}_B , \mathbf{n}_{gc} , and \mathbf{n}_w unchanged, quite remarkably, it also has no direct role in influencing the eigendirections of \mathbf{S} , as seen from equation 5. However, compressible modes could lead to *indirect* effects on the eigendirections, due to changes in the local amplitudes of the pressure, \mathbf{B} , $\boldsymbol{\omega}$, and the strain eigenvalues. That the alignments remain qualitatively unchanged suggests that such effects are minor. Furthermore, the fact that the PDFs obtained from the ideal $\mathcal{M} = 0.3$ are qualitatively similar to the non-ideal run implies that molecular dissipation does not play a direct role in determining the qualitative nature of the alignments discussed here. However, a full quantitative prediction for the statistics of various angles would require an examination of the dissipation rates of \mathbf{B} , $\boldsymbol{\omega}$ and ∇C in each eigen direction of \mathbf{S} following the method of Nomura & Post (1998).

In the kinematic phase, the orientations of \mathbf{n}_{gc} and \mathbf{n}_w are consistent with previous results for hydrodynamical flows (Kerr 1987; Ashurst et al. 1987; Sreenivasan & Antonia 1997). The scalar gradient is strongly aligned with \mathbf{e}_γ , the only compressive direction of the strain, and thus orthogonal to the directions in which stretching occurs. The vorticity lies preferentially in the \mathbf{e}_α - \mathbf{e}_β plane, where the strain is extensive, but is more strongly-aligned with the intermediate eigenvector \mathbf{e}_β rather than the principal eigenvector, \mathbf{e}_α (Kerr 1987; Ashurst et al. 1987). Although vorticity is produced primarily along \mathbf{e}_α , the angle between \mathbf{n}_w and \mathbf{e}_α shows a rather uniform distribution, because vorticity is converted to the direction \mathbf{e}_β due to a rotation of the eigenvectors by the off-diagonal components in equation 5 (Nomura & Post 1998). For example, the $\boldsymbol{\omega}_\alpha \boldsymbol{\omega}_\beta$ term causes a rotation of \mathbf{e}_α and \mathbf{e}_β that leads to a preferential alignment of $\boldsymbol{\omega}$ with \mathbf{e}_β (She et al. 1991). Finally, the direction of \mathbf{B} relative to the eigenvectors is similar to $\boldsymbol{\omega}$ due to the similarity of their equations in the kinematic phase, although a difference exists in their PDFs with \mathbf{e}_α , which may be caused by the vorticity term in equation 1 for \mathbf{B} . The fact that the magnetic field in the kinematic phase lies in the \mathbf{e}_α - \mathbf{e}_β plane dates back to the earlier analytic studies of Zel'dovich et al. (1984); Chertkov et al. (1999);

Schekochihin & Cowley (2007).

In the saturated phase, the alignments of \mathbf{n}_B , \mathbf{n}_{gc} , and \mathbf{n}_ω , with \mathbf{e}_β are qualitatively similar to those in the kinematic phase, but there are notable changes in the PDFs with the other two eigenvectors, especially for \mathbf{n}_B and \mathbf{n}_{gc} . The peak of the PDF for \mathbf{n}_B with \mathbf{e}_α shifts from 0° to $\approx 45^\circ$ and the peak for \mathbf{n}_B with \mathbf{e}_γ shifts from 90° to $\approx 55^\circ$, as also reported in (Brandenburg et al. 1995; Brandenburg 1995). Not measured before is the shift of the peak of the PDF of \mathbf{n}_{gc} with \mathbf{e}_α from 90° to $\approx 60^\circ$ and that of \mathbf{n}_{gc} with \mathbf{e}_γ from 0° to $\approx 30^\circ$. These changes suggest a rotation of \mathbf{e}_α and \mathbf{e}_γ by \mathcal{L} , which can occur through the off-diagonal component, $\mathcal{L}_{\alpha\gamma}$, in an equation similar to equation 5. As \mathbf{L} does not directly act on \mathbf{B} and ∇C , it would not affect the tendency of \mathbf{n}_{gc} to align perpendicularly to \mathbf{n}_B (Figure 2).

Unlike \mathbf{n}_B and \mathbf{n}_{gc} , no peak shift is observed in the PDFs of the \mathbf{n}_ω relative to the eigenvectors, except for a slightly stronger anti-correlation with \mathbf{e}_α . Note that unlike \mathbf{B} and ∇C , the Lorentz force acts directly on the vorticity (equation 3), and the direction change of $\boldsymbol{\omega}$ by $\nabla \times \mathbf{L}$ appears to roughly compensate the rotation of the eigenvectors by the off-diagonal components of \mathcal{L} . Thus, as the magnetic strength increases and saturates, the alignment of \mathbf{n}_ω with the eigenvectors remains largely unchanged. A consequence of \mathbf{L} directly acting on $\boldsymbol{\omega}$ but not on \mathbf{B} and ∇C is a weaker alignment of \mathbf{n}_ω with \mathbf{n}_B and a weaker transverse correlation of \mathbf{n}_ω with \mathbf{n}_{gc} in the saturated phase.

The weaker alignment of ∇C with \mathbf{e}_γ in the saturated phase has important consequences for mixing, as it leads to a slower amplification of the scalar gradient. The Lorentz force also opposes the compressive motion of the strain, and decreases the amplitude of the compressive eigenvalue, which further decrease the mixing rate. In fact, in simulations with an isotropic κ , mixing was found to be suppressed in the saturated phase Sur et al. (2014). Furthermore, the orthogonality of \mathbf{B} and ∇C at all times implies that in a medium with anisotropic κ , mixing is likely to be suppressed even in the kinematic phase.

3.3. Overview

Taken together, the features of the various alignments described here lead to the following coherent physical picture. For simplicity, we consider the incompressible case in which a compressive motion is in the $\hat{\mathbf{x}}$ direction and the extensive motions occur in the $\hat{\mathbf{y}}\text{-}\hat{\mathbf{z}}$ plane. In the kinematic phase, this will - (i) increase the concentration gradient in $\hat{\mathbf{x}}$ and decrease it in the other directions, (ii) increase the magnetic field in $\hat{\mathbf{y}}$ and $\hat{\mathbf{z}}$, and decrease it in $\hat{\mathbf{x}}$ because of flux freezing, and (iii) increase the vorticity in $\hat{\mathbf{y}}$ and $\hat{\mathbf{z}}$, and decrease it in $\hat{\mathbf{x}}$, because of angular momentum conservation. In the saturated phase, a substantial Lorentz force, \mathbf{L} , develops, which rotates $\boldsymbol{\omega}$ and the eigenvectors of the strain. The directions of \mathbf{B} and ∇C are not directly affected by \mathbf{L} , and therefore they remain largely orthogonal. However, the Lorentz force tends to be aligned with ∇C , thereby resisting

the compressive motion of the strain, leading to slower mixing. More detailed analysis of the Lorentz force and its effect on $\boldsymbol{\omega}$ and the strain tensor, and the dissipation rates of \mathbf{B} , ∇C , and $\boldsymbol{\omega}$ in the eigendirections of \mathcal{S} will provide further insight into the coevolution of magnetic field growth and scalar mixing in the presence of turbulence.

SS & ES were supported by the National Science Foundation under grant AST11-03608 and NASA theory grant NNX09AD106. LP acknowledges support from the Clay postdoctoral fellowship at Harvard-Smithsonian Center for Astrophysics. The authors would also like to acknowledge the Advanced Computing Center at Arizona State University (URL: <http://a2c2.asu.edu/>), the Texas Advanced Computing Center (TACC) at The University of Texas at Austin (URL: <http://www.tacc.utexas.edu>), and the Extreme Science and Engineering Discovery Environment (XSEDE) for providing HPC resources via grant TG-AST130021 that have contributed to the results reported within this paper. The FLASH code is developed in part by the DOE-supported Alliances Center for Astrophysical Thermonuclear Flashes (ASC) at the University of Chicago.

REFERENCES

- Ashurst, W. T., Kerstein, A. R., Kerr, R. M., & Gibson, C. H. 1987, *Physics of Fluids*, 30, 2343
- Becker, G. D., Rauch, M., & Sargent, W. L. W. 2009, *ApJ*, 698, 1010
- Bhat, P., & Subramanian, K. 2013, *MNRAS*, 429, 2469
- Brandenburg, A. 1995, *Chaos Solitons and Fractals*, 5, 2023
- Brandenburg, A., Nordlund, A., Stein, R. F., & Torkelsson, U. 1995, *ApJ*, 446, 741
- Brandenburg, A., Sokoloff, D., & Subramanian, K. 2012, *Space Sci. Rev.*, 169, 123
- Brandenburg, A., & Subramanian, K. 2005, *Phys. Rep.*, 417, 1
- Chertkov, M., Falkovich, G., Kolokolov, I., & Vergassola, M. 1999, *Physical Review Letters*, 83, 4065
- Cho, J., & Ryu, D. 2009, *ApJ*, 705, L90
- Cho, J., Vishniac, E. T., Beresnyak, A., Lazarian, A., & Ryu, D. 2009, *ApJ*, 693, 1449
- Federrath, C., Chabrier, G., Schober, J., et al. 2011, *Physical Review Letters*, 107, 114504
- Fryxell, B., Olson, K., Ricker, P., et al. 2000, *ApJS*, 131, 273
- Haugen, N. E., Brandenburg, A., & Dobler, W. 2004, *Phys. Rev. E*, 70, 016308
- Kerr, R. M. 1987, *Physical Review Letters*, 59, 783
- Komarov, S. V., Churazov, E. M., Schekochihin, A. A., & Zuhone, J. A. 2014, *MNRAS*, arXiv:1304.1857
- Lee, D. 2013, *Journal of Computational Physics*, 243, 269
- Lee, D., & Deane, A. E. 2009, *Journal of Computational Physics*, 228, 952
- Miyoshi, T., & Kusano, K. 2005, *Journal of Computational Physics*, 208, 315
- Miller, R. S., Mashayek, F., Adumitroaie, V., & Givi, P. 1996, *Physics of Plasmas*, 3, 3304
- Nomura, K. K., & Post, G. K. 1998, *Journal of Fluid Mechanics*, 377, 65
- Pan, L., & Scalo, J. 2007, *ApJ*, 654, L29
- Pan, L., & Scannapieco, E. 2010, *ApJ*, 721, 1765

- Pan, L., Scannapieco, E., & Scalo, J. 2013, ArXiv e-prints, arXiv:1306.4663
- Pichon, C., Scannapieco, E., Aracil, B., et al. 2003, ApJ, 597, L97
- Pieri, M. M., Schaye, J., & Aguirre, A. 2006, ApJ, 638, 45
- Scannapieco, E., Pichon, C., Aracil, B., et al. 2006, MNRAS, 365, 615
- Schaye, J., Aguirre, A., Kim, T.-S., et al. 2003, ApJ, 596, 768
- Schekochihin, A. A., & Cowley, S. C. 2007, Turbulence and Magnetic Fields in Astrophysical Plasmas, ed. S. Molokov, R. Moreau, & H. K. Moffatt (Springer), 85
- Schekochihin, A. A., Cowley, S. C., Taylor, S. F., Maron, J. L., & McWilliams, J. C. 2004, ApJ, 612, 276
- She, Z.-S., Jackson, E., & Orszag, S. A. 1991, Royal Society of London Proceedings Series A, 434, 101
- Shraiman, B. I., & Siggia, E. D. 2000, Nature, 405, 639
- Sreenivasan, K. R., & Antonia, R. A. 1997, Annual Review of Fluid Mechanics, 29, 435
- Sur, S., Pan, L., & Scannapieco, E. 2014, ApJ, 784, 94
- Zel'dovich, Y. B., Ruzmaikin, A. A., Molchanov, S. A., & Sokolov, D. D. 1984, Journal of Fluid Mechanics, 144, 1